

Statistical analysis of the distribution of gold particles over antigen sites after immunogold labelling

C.A. Glasbey

Biomathematics and Statistics Scotland

JCMB, King's Buildings, Edinburgh, EH9 3JZ, Scotland

and I.M. Roberts

Unit of Transport Processes

Department of Cellular and Environmental Physiology

Scottish Crop Research Institute

Invergowrie, Dundee DD2 5DA, Scotland

Abstract

The locations of immunogold labelled particles on ultrathin sections of pellets of purified tobacco rattle virus were analysed statistically. The distributions were found to be inconsistent with a Poisson process. Instead, a physically-based model, a modified Poisson process, is proposed and shown to fit the data well. The antigen sites to which antibodies are attached are assumed to follow a Poisson process and one gold particle sits on top of each site. However, if two sites are closer than a threshold then the physical size of the gold particles with attached antibodies pushes the particles apart, and if sites are nearer than a higher threshold there is a chance that surface tension will pull the gold particles together.

Key words: K-function, Poisson process, Stochastic point process.

1 Introduction

Immunogold labelling (IGL) of ultrathin sections is a powerful technique for the detection of antigens in samples of embedded tissues. It depends entirely on the exposure of antigen/epitope sites on the surface of the section which are then recognised by antibodies which are coupled to particles of colloidal gold. However, the number of potential labelling sites available for IGL bears little relationship to the number of visible antigens where the antigen has a recognizable form e.g. plant viruses (Fig 1), because (a) most of the particles seen in sections are below the

surface and are therefore unavailable for labelling (van Lent *et al.*, 1990) and (b) because not all antigen sites on the surface of the section are antigenic. Previous work to optimise the conditions for gold labelling was successful (Roberts, 1994), but at that time, no effort was made to analyse the distribution of the gold particles, other than to try to correlate the label density to the virus particle concentration and orientation within the section. This paper describes such an analysis .

Tobacco rattle virus, PRN isolate (TRV-PRN), (Harrison and Woods, 1966) was purified and pelleted by high-speed centrifugation. After ultracentrifugation of the virus extract, the supernatant was discarded and the virus pellet was embedded in Araldite resin (Ciba-Geigy) as described by Roberts (1994). Ultrathin sections (silver/gold interference colours) were cut on a Reichert Ultracut E ultramicrotome with tungsten-coated glass knives (Roberts, 1975), heat-stretched (Roberts, 1970) and mounted on pyroxylin-filmed nickel grids (hexagonal 200 mesh).

Polyclonal IgG from rabbit antisera was prepared as described by Fasseas *et al.*, (1989), and cross-absorbed before use (Roberts, 1994). The IgG was used at a concentration of 10 $\mu\text{g}/\text{ml}$ and all dilutions of IgG and gold probe were made in IGL buffer (Fasseas *et al.*, 1989). Attempts to use IgG Fab fragments, to increase the gold label density and thus assess the importance of the length of the antibody molecule, were unsuccessful. The gold probe used in all experiments was gold-conjugated goat anti-rabbit IgG (GARG) (15 nm) (Amersham International) at a dilution of OD520 = 0.5 in IGL buffer. The labelling procedure was as described by Roberts (1994). After IGL, the grids were stained with uranyl acetate followed by lead citrate, and examined in a Philips CM10 or a JEOL 100S electron microscope.

Ascertaining whether the points in Fig 1 are distributed totally at random, or in accord with some model, can aid the understanding of IGL. The statistical analysis of spatial point patterns has a well developed methodology dating back to the 1970s (see the very readable monograph of Diggle, 1983). For more recent references, see Stoyan *et al.* (1995). In the following section we will first test for complete randomness, and then develop a physically-based model to explain the distribution of gold particles.

2 Statistical analysis

The first question which is usually addressed in the analysis of point patterns is whether the distribution is consistent with complete randomness, the so-called Poisson process. Konig *et al.* (1991) reviewed methods for analysing 3-D arrangements of particles, such as the locations of cell nuclei obtained using a confocal scanning light-microscope. We have based our analysis on Diggle (1983, chapter 2). He discusses ways of extracting summary statistics from 2-D spatial point data, which reveal aspects of their pattern. In particular, he recommends two distributions:

- the probability distribution of the distance from a point in the data set to the nearest other point, where $G(y)$ denotes the probability that this distance is $\leq y$;

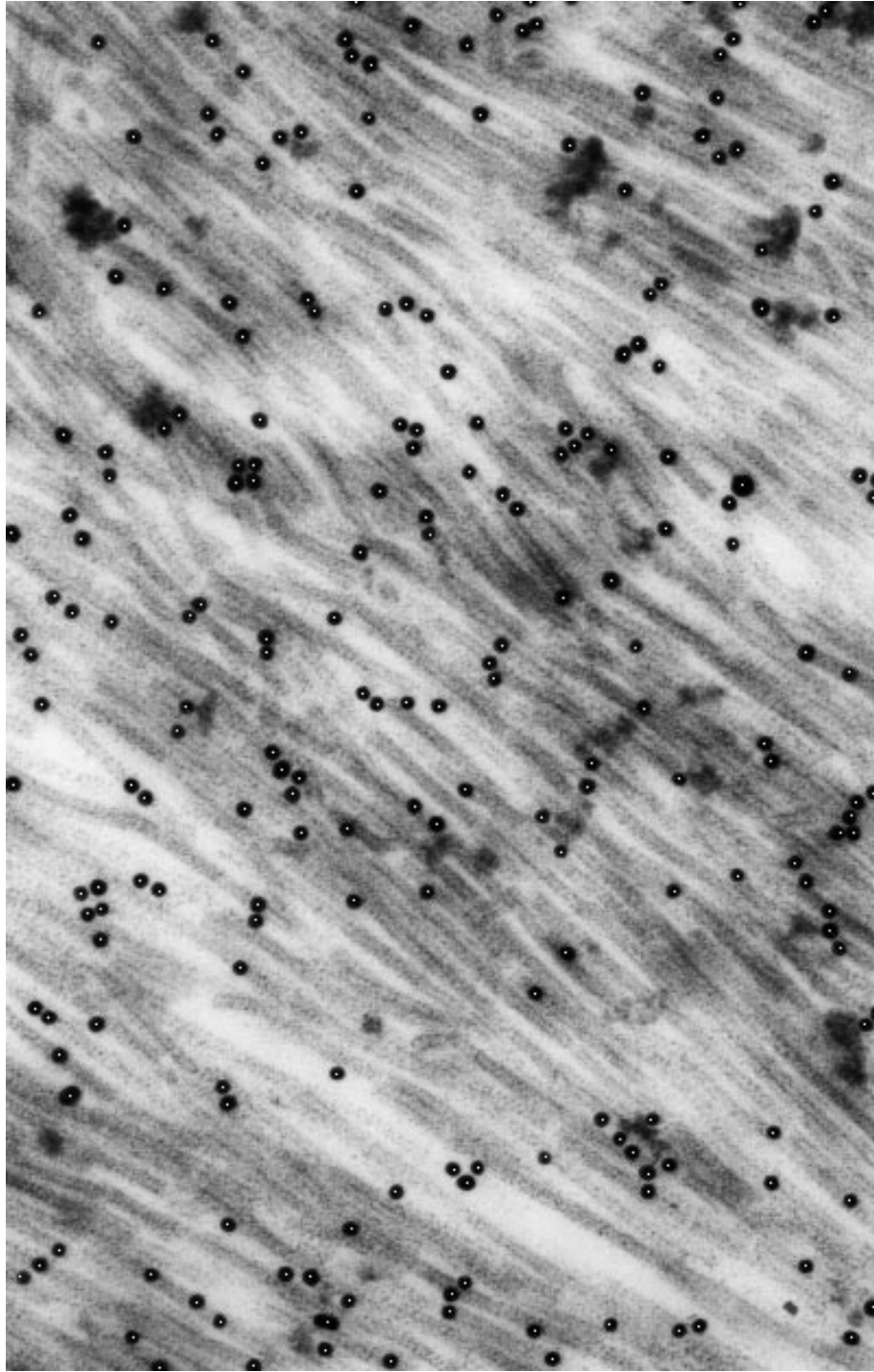


Figure 1: *Ultrathin section of a pellet of purified tobacco rattle virus after IGL with goat anti-rabbit gold (15nm) probe (from Fig 3(b) of Roberts, 1994). Centres of the 218 gold particles are indicated by white points.*

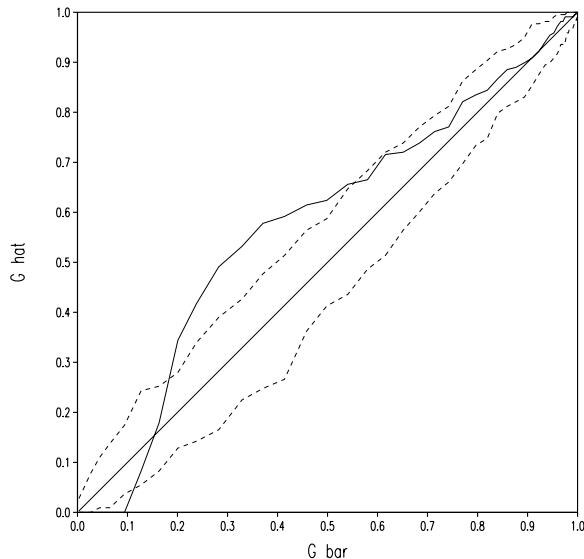


Figure 2: \hat{G} for points in Fig 1 plotted against the expected values for a Poisson process (—) obtained as the average (\bar{G}) of 99 simulations, together with the 45° line and the envelope of estimates of G for 99 simulations from a Poisson process (- - -).

- the probability distribution of the distance from any location in the region of interest (the sampled rectangle) to the nearest point in the data set, where $F(y)$ denotes the probability that this distance is $\leq y$;

These cumulative distribution functions can be estimated from the data. The continuous line in Fig 2 shows \hat{G} for the 218 points in Fig 1, plotted against their expected values for a Poisson process. The expected values were obtained by averaging results from 99 simulations of 218 random points, denoted \bar{G} . \hat{G} should lie close to the 45° line, which is also plotted, although sampling variation means that it will not coincide exactly with this line. The dashed lines show the envelope of estimates of G for 99 simulations from a Poisson process, i.e., the lines from all 99 simulations lie between the dashed lines. \hat{G} passes outside this envelope and is therefore more extreme than any of the 99 simulations, so we should reject the Poisson process as a model for the data. The test can be formalised, e.g. using as a test statistic the integrated squared difference between \hat{G} and \bar{G} :

$$\int_0^{\infty} \{ \hat{G}(y) - \bar{G}(y) \}^2 dy .$$

This statistic gives a value for Fig 2 which is beyond the range of values obtained for a Poisson process, confirming that we should reject this model at the 1% level.

We now address the question of what model is compatible with the data. It makes sense to use any available knowledge of the processes generating the data, because otherwise it is almost certainly impossible to unambiguously select a model. We know two physical facts:

1. gold particles with attached antibodies have a physical size, so their effective centres cannot be arbitrarily close together;
2. surface tension forces during the drying process can pull gold particle/antibody complexes together if their anchor points are not too far apart, in a manner analogous to the clumping of spherical particles on a substrate during air drying (Roberts and Duncan, 1981). The model, therefore, can be likened to a ‘ball and chain’, where the shackle represents the anchor point, the chain is the rabbit/goat anti-rabbit IgG binding complex, and the ball is the colloidal gold particle.

Diggle (1983, chapter 4) recommends the use of the K function to identify and fit models to data. $K(t)$ is defined to be the expected number of points within distance t of a particular point, divided by the average number of points per unit area. Therefore, for the Poisson process where points are distributed totally at random, $K(t) = \pi t^2$, i.e. $K(t)$ is simply the area of a circle of radius t . The continuous line in Fig 3(a) shows $\sqrt{\hat{K}(t)}$ plotted against t for the points in Fig 1, together with the straight line $\sqrt{\pi t}$ plotted against t , from which we can see both effects 1 and 2. (Note that, \hat{K} has been adjusted for edge effects, as described in Diggle (1983, chapter 5).) Effect 1 results in $\hat{K}(t)$ being zero for $t < 10$ nm, and effect 2 causes $\sqrt{\hat{K}(t)}$ to exceed $\sqrt{\pi t}$ over the range $15 \text{ nm} < t < 45 \text{ nm}$.

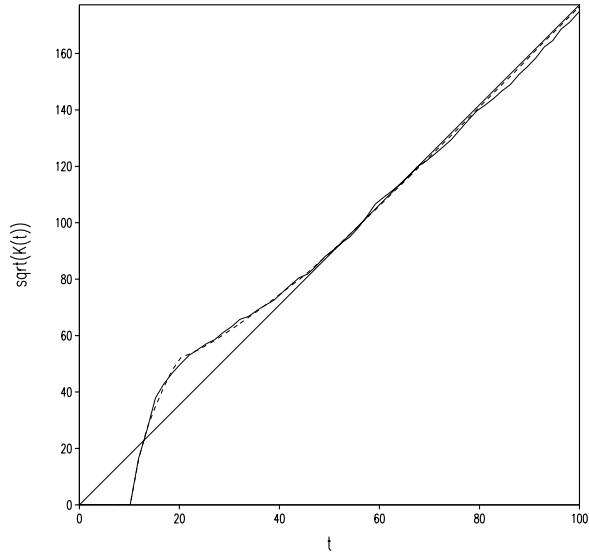
We propose the following model:

- the anchor points, i.e., the antigen sites to which antibodies are attached, are distributed according to a Poisson process,
- one gold particle sits on top of each anchor point, except that:
 1. if two gold particles are closer together than a threshold distance D_1 they are pushed apart to a distance which is uniformly distributed between D_1 and another distance, D_2 ;
 2. if the distance (D) to the nearest gold particle is in the range D_1 to a third distance, D_3 , then with probability

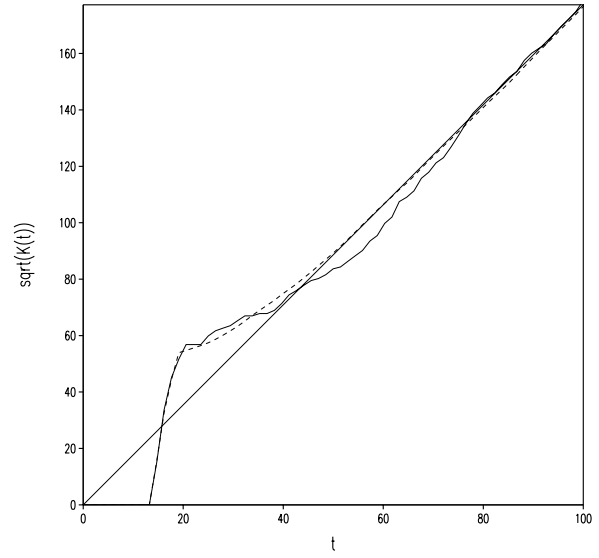
$$\frac{D_3 - D}{D_3 - D_1}$$

the particles are drawn together to a distance which is again uniformly distributed between D_1 and D_2 . Therefore, if $D = D_1$ the particles are moved with probability 1, if $D = D_3$ they are moved with probability 0, and in between the probability changes linearly.

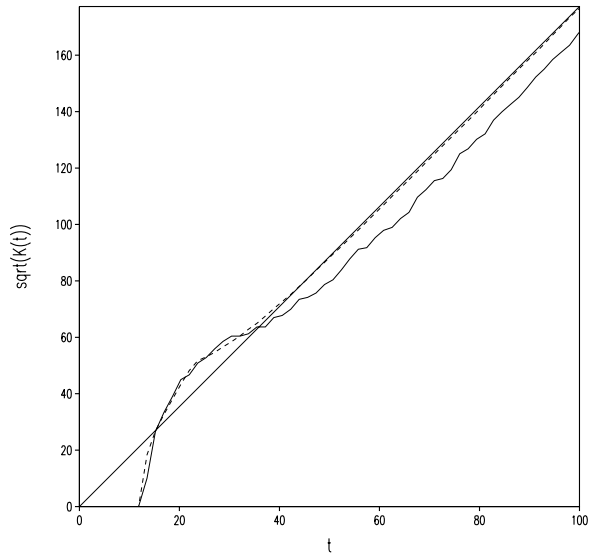
The gold particles vary in size, and D_1 and D_2 represent the range of values of the lower limit of inter-particle distances. D_3 corresponds to the combined lengths of two rabbit/goat anti-rabbit IgG binding complexes, which is the upper limit for the distance between two anchor points such that the particles can touch. We have assumed that distributions are uniform. It would have been possible to choose alternative distributions, such as the Gaussian, and a different monotonically decreasing function of D , but the data are probably not sufficient to



(a)



(b)



(c)

Figure 3: $\sqrt{\hat{K}(t)}$ plotted against t nm (—), together with the straight line $\sqrt{\pi t}$ plotted against t (—), and expected K values for the fitted model (- - -): **(a)**: for points in Fig 1, **(b)**: for points in Fig 1(b) of Roberts (1994), **(c)**: for points in Fig 2(a) of Roberts (1994).

data set	\hat{D}_1	\hat{D}_2	\hat{D}_3
a	10.9	19.8	54.0
b	14.3	19.2	52.0
c	12.0	23.2	43.3

Table 1: *Estimated parameter values (nm) in point process model for three data sets.*

data set	G	F
a	72	23
b	90	93
c	82	1

Table 2: *Percentage significance levels for \hat{G} and \hat{F} for the fitted models.*

discriminate between models to this level of detail. Note that, in simulating the point process it is sometimes necessary to move a particle more than once to ensure that conditions 1 and 2 are both satisfied.

The model requires three parameters, D_1 , D_2 and D_3 , which can be estimated by minimising

$$\sum_t \left\{ \hat{K}(t)^{0.25} - K(t)^{0.25} \right\}^2$$

where the summation is over values of t up to one quarter of the width of the image and $K(t)$ is a function of D_1 , D_2 and D_3 (Diggle, 1983, chapter 5). No closed form expression is available for $K(t)$ for our model, so it had to be obtained by simulation. We used 1000 simulations from the point process model, and found optimal values for the parameters using the Nelder-Mead simplex method (NAG, 1993). The dashed line in Fig 3(a) shows \sqrt{K} for the best fitting model, which show remarkably close agreement with the data. The corresponding parameter estimates are given in the first row of Table 1.

The model was fitted to two further data sets in Roberts (1994), namely his Figs 1(b) and Fig 2(a). Observed and fitted K functions are plotted in Figs 3(b) and (c), and parameter estimates are given in Table 1. The agreement with the data is good, although not quite as good as in Fig 3(a). Parameter estimates show reasonable consistency between data sets and with values to be expected from physical considerations.

The fit of the point process model was tested by comparing observed G and F distributions with their expected values, as we did earlier for the Poisson process. Probability levels are given in Table 2, i.e., the number of simulations for which the statistic exceeded the one for the observed pattern. Only one is significant, the F distribution for data set (c), confirming that in general the model agrees well with the data.

3 Discussion

Irrespective of any variations in the embedding or labelling protocols to improve the labelling efficiency, the label density over the sections will always be low compared with the numbers of virus particles visible. The antigenic mass of viruses is low (Beesley, 1984) which in turn leads to the binding of few antibody molecules and thus low particle labelling (Oram and Crooks, 1979). Also, most of the virus particles seen in sections are below the surface and are unavailable for labelling (van Lent *et al.*, 1990), and, in addition, there may be steric hindrance of the gold probes of any surface epitopes (Hyatt *et al.*, 1988). Furthermore, when tissues are processed for electron microscopy, there is considerable distortion and shrinkage during fixation and dehydration (Boyde and Boyde, 1980; Boyde and Maconnachie, 1981) and this may alter the antigen epitope sites, thus preventing recognition and attachment of the labelling antibody. All these factors will, consequently, contribute to the relative paucity of gold particle/antibody/antigen sites on the section surface. It seems unlikely, therefore, that steric hindrance will have a significant role in the separation distances between the gold particles, or that the low numbers of gold particles will affect the analysis of their distribution.

Rusakov *et al.* (1995) analysed the co-localisation of immunogold double-labelled neural cell adhesion molecule isoforms in chick forebrain. They found that antibodies against alpha 2,8 polysialic acid (PSA) tended to form clusters, although no mention is made as to whether the gold conjugate was monodisperse. Small clusters of gold are commonly found on IGL sections but are usually indicative of a breakdown in the conjugate, thus allowing the gold particles to aggregate. In our study, there was very little evidence of a ‘micro-precipitate’, and so we took no account of it in our analysis. For data where it occurs more frequently, the effect should be included in the point process model. Our results do show, however, that the distribution of gold particles is inconsistent with a Poisson process. We show that a physically-based model, a modified Poisson process, fits the data well. This involves assuming that the antigen sites follow a Poisson process, with one gold particle sitting on top of each site. But, if two sites are closer than a threshold, then the particles are pushed apart, and if sites are nearer than a higher threshold, surface tension pulls them together.

Acknowledgements

The work was supported by funds from the Scottish Office Agriculture, Environment and Fisheries Department.

References

Beesley, J.E. (1984). Recent advances in microbiological immunocytochemistry. In: *Immunolabelling for Electron Microscopy* (Polak, J.M. and Varndell, I.M. eds.) pp 289-303. Elsevier, Amsterdam.

- Boyde, A. and Boyde, S. (1980). Further studies of specimen volume changes during processing for SEM, including some plant tissue. *Scanning Electron Microsc.* **2**, 117-124.
- Boyde, A. and Maconnachie, E. (1981). Morphological correlations with dimensional change during SEM specimen preparation. *Scanning Electron Microsc.* **4**, 27-34.
- Diggle, P.J. (1983). *Statistical Analysis of Spatial Point Patterns*. Academic Press, London.
- Fasseas, C., Roberts, I.M. and Murant, A.F. (1989). Immunogold localisation of parsnip yellow fleck virus particle antigen in thin sections of plant cells. *J. gen. Virol.* **70**, 2741-2749.
- Harrison, B.D. and Woods, R.D. (1966). Serotypes and particle dimensions of tobacco rattle viruses from Europe and America. *Virology* **28**, 610-620.
- Konig, D., Carvajal-Gonzalez, S., Downs, A.M., Vassy, J. and Rigaut, J.P. (1991). Modeling and analysis of 3-D arrangements of particles by point-processes with examples of application to biological data obtained by confocal scanning light-microscopy. *J. Microscopy* **161**, 405-433.
- Hyatt, A.D., McPhee, D.A. and White, J.R. (1988). Antibody competition studies with gold-labelling immunoelectron microscopy. *J. Virol. Methods* **19**, 23-32.
- Numerical Algorithms Group (1993). *Library Manual Mark 16*. NAG Central Office, 256 Banbury Road, Oxford OX2 7DE, UK.
- Oram, J.D. and Crooks, A.J. (1979). A comparison of labelled antibody methods for the detection of virus antigens in cell monolayers. *J. Immunol. Methods* **25**, 297-310.
- Roberts, I.M. (1970). Reduction of compression artifacts in ultrathin sections by the application of heat. *J. Microscopy* **92**, 57-61.
- Roberts, I.M. (1975). Tungsten coating - a method of improving glass microtome knives for cutting ultrathin sections. *J. Microscopy* **103**, 113-119.
- Roberts, I.M. and Duncan, G.H. (1981). A simple device for freeze-drying electron microscope specimens. *J. Microscopy* **124**, 295-303.
- Roberts, I.M. (1994). Factors effecting the efficiency of immunogold labelling of plant virus antigens in thin sections. *J. Virol. Methods* **50**, 155-166.
- Rusakov, D.A., Davies, H.A., Stewart, M.G. and Schachner, M. (1995). Clustering and co-localization of immunogold double labelled neural cell adhesion molecule isoforms in chick forebrain. *Neuroscience Letters* **183**, 50-53.
- Stoyan, D., Kendall, W.S. and Mecke, J. (1995). *Stochastic Geometry and its Applications (2nd edition)*. Wiley, Chichester.
- van Lent, J.W.M. (1988). *Localisation of viral antigens in leaf protoplasts and plants by immunogold labelling*. Ph.D. Thesis, Agricultural University, Wageningen, The Netherlands.

van Lent, J.W.M., Wellink, J. and Goldbach, R. (1990). Evidence for the involvement of the 58K and 48K proteins in the intercellular movement of cowpea mosaic virus. *J. gen. Virol.* **71**, 219-223.